Optimal combination of data modes in inverse problems: maximum compatibility estimate

Mikko Kaasalainen
Dept. of Mathematics
Tampere UT

- Case study of complementary data modes: generalized projections
- Major mode: volumes of projections
- Minor mode: boundary curves of projections
- Solution: shape and spin state
- Astrophysical data: photometry and adaptive optics (AO)
- AO processing an inverse problem itself
- Brightness distribution $I(u)$, $u \in \mathbb{R}^2$ from AO deconvolution unreliable and prone to large contrast errors
- Boundary $\partial\mathcal{D}$, $\mathcal{D} = \{u : I(u) > \epsilon\}$ **much** more accurate
- With $\partial\mathcal{D}$, no modelling of the scattering properties of the surface required (and solution from volume data insensitive to scattering)

LC + AO: consistency

- AO images and LC models are both solutions of inverse problems
- AO images agree well with independent LC-based models, so…
- …we can expect a joint model to fit data from both sources well (not necessarily always the case, esp. with LCs+ delay-Doppler radar)

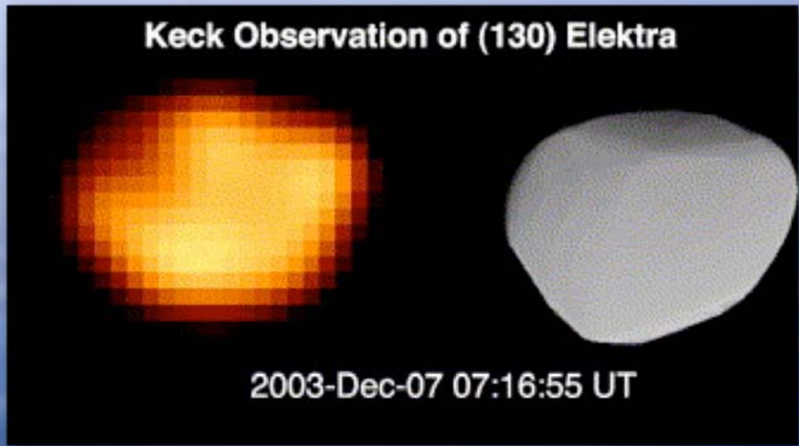

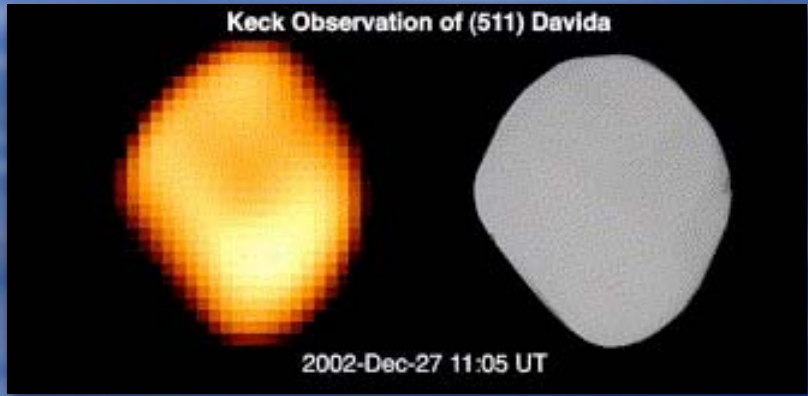

Multidatainversion

- Minimize a joint χ^2 such that separate AO and LC χ^2s are acceptable
- e.g.: (9) Metis with a strong smoothness constraint to suppress too many artificial details
- But one AO image suggests a large crater/spot: let's just add it and see what happens...

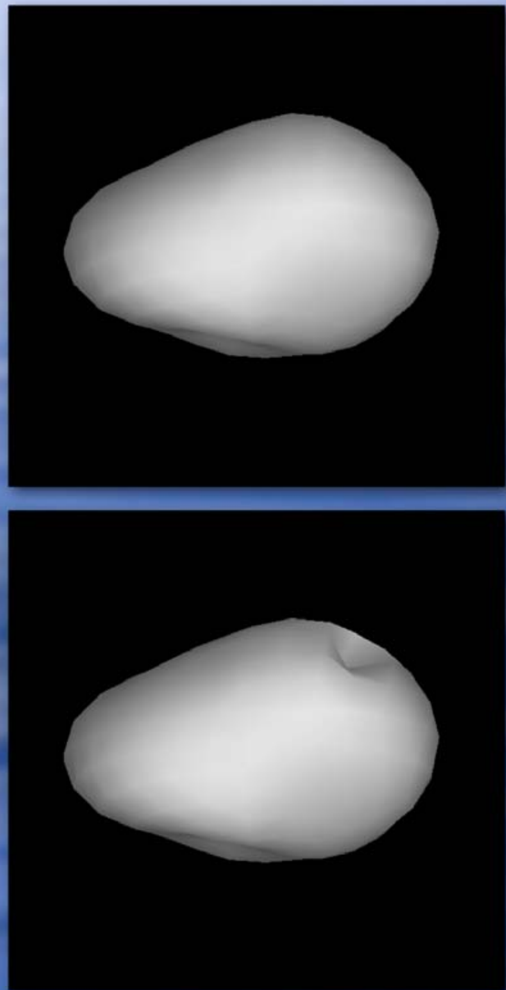

Is it there...

- The AO spot can be reproduced with a suitable crater (left)...
- ...but then it should also be seen in other images (right)!
- AO post-processing tends to produce exaggerated contrasts and spurious "features"

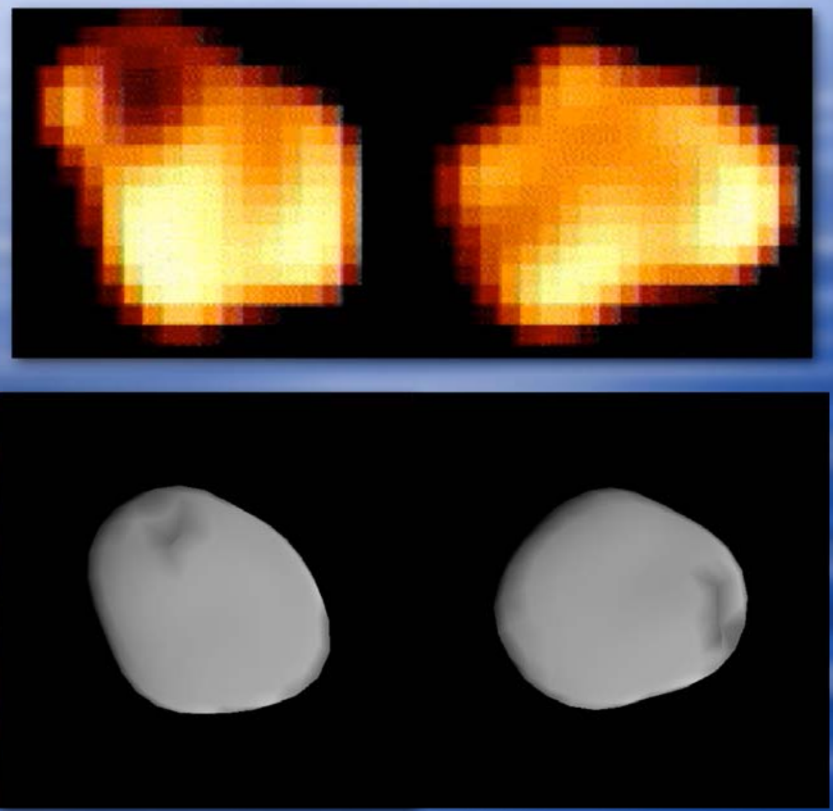

...or not?

- No spot seen in original basic-processed AO images -- better to err on the safe side
- Post-processing (from basic image and estimated PSF) is always nonunique: it uses selected a priori constraints not necessarily mutually consistent with the full shape/spin model

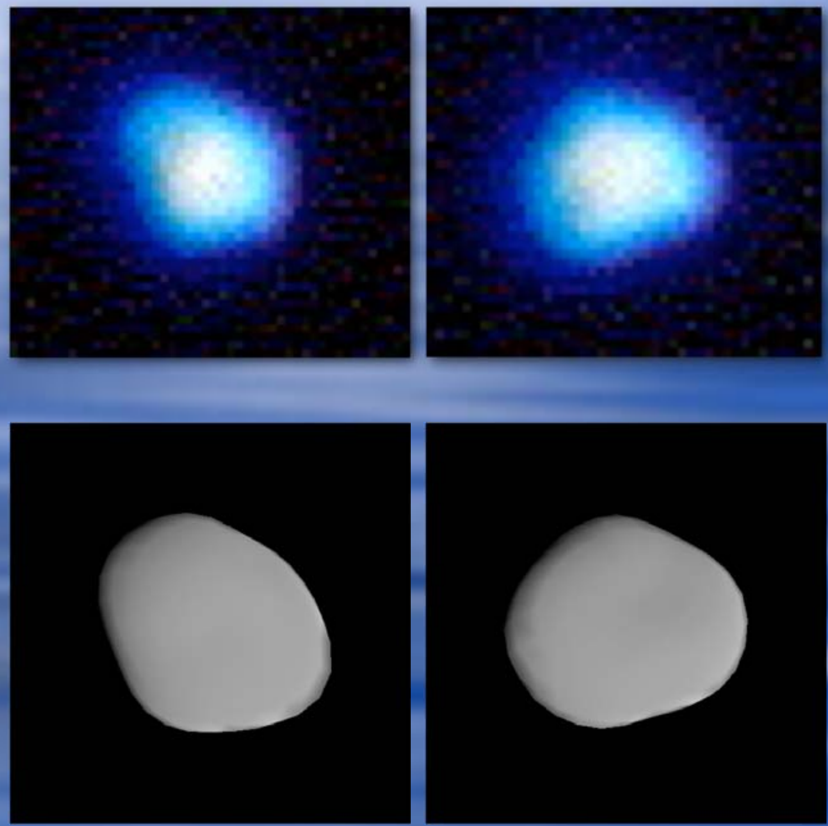

The art of a priori info

- In principle, the 3-D model should enter already at the post-processing stage: we could invert basic AO+PSF+LC data
- But post-processing seems to produce very good/sharp edges (silhouette), so we should invert post-proc edges+LC data...
- ...work in progress: how to get maximal reliable info and separate true details from artificial ones, and how to keep “only” those details in the model

1 Profiles, TCBs, uniqueness

- Volumes of projections: unique solution for convex bodies $\mathcal{C}$
- Profiles (silhouettes): unique for tangent-covered bodies $\mathcal{T}$
- Generalized profiles (shadows included): unique for a larger class $\mathcal{G}$

$$\mathcal{C} \subset \mathcal{T} \subset \mathcal{G}.$$

Profile of $\mathcal{B}$ in direction $\omega \in S^2$:

$$\mathcal{P}_\partial(\omega, \mathcal{B}) = \partial\mathcal{P}(\omega, \mathcal{B})$$

Cylinder continuation of a set of points $\mathcal{S}$ in direction ω:

$$\mathcal{C}(\omega, \mathcal{S}) = \left\{ x + s\omega \middle| x \in \mathcal{S}; -\infty < s < \infty \right\}. \tag{1}$$

Profile hull is formed by several profiles:

$$\mathcal{H}(\{\mathcal{P}_\partial(\omega_i)|_{i=1}^{N}\}) = \partial \bigcap_i \mathcal{C}(\omega_i, \mathcal{S}_i), \quad \mathcal{S}_i = \left\{ x_\varkappa(\omega_i) \middle| \varkappa \in \mathcal{P}(\omega_i) \right\}. \tag{2}$$

Condition for correct profile offsets: the profiles of the constructed $\mathcal{H}$ must be identical to the observed ones.

$$\mathcal{P}_\partial[\omega_i, \mathcal{H}(\{\mathcal{P}_\partial(\omega_j)|_{j=1}^{N}\})] = \mathcal{P}_\partial(\omega_i)$$

Tangent-covered bodies (TCBs) are bodies that are their own complete profile hulls: $\mathcal{B} = \mathcal{H}_C(\mathcal{B})$. Thus, each surface point $x \in \mathcal{B}$ of a TCB is mapped at least to one $\mathcal{P}_\partial(\omega)$.

Generalized profiles: illumination and viewing directions $(\omega_0, \omega) \in S^2 \times S^2$ define the region

$$\mathcal{A}_+(\omega, \omega_0; \mathcal{B}) = \mathcal{A}_+(\omega; \mathcal{B}) \cap \mathcal{A}_+(\omega_0; \mathcal{B}), \tag{3}$$

where

$$\mathcal{A}_+(\omega; \mathcal{B}) = \left\{ x \in \mathcal{B} \middle| \langle \nu(x), \omega \rangle \geq 0; \forall s > 0 : x + s\omega \notin \mathcal{B} \right\}, \tag{4}$$

where $\nu(x)$ is the unit surface normal at x. The projection $\mathcal{P}$ of the boundary $\partial \mathcal{A}_+$ is now the generalized profile:

The *generalized profile* of the body $\mathcal{B}$ in the direction ω and at illumination direction ω_0 is

$$\partial \mathcal{P}[\omega, \mathcal{A}_+(\omega, \omega_0; \mathcal{B})] = \mathcal{P}[\omega, \partial \mathcal{A}_+(\omega, \omega_0; \mathcal{B})]. \tag{5}$$

Uniqueness theorems for reconstructions from generalized profiles can be shown for various configurations; e.g., shadow contours of a known part $\mathcal{K}$ of $\mathcal{B}$ on an unknown part $\mathcal{U}$, or shadow contours of $\mathcal{U}$ on $\mathcal{K}$.

2 Combined data modes

Full χ^2:

$$\chi^2_{\rm tot} = \chi^2_L + \lambda_\partial \chi^2_\partial + \lambda_R g(P), \tag{6}$$

Volume of generalized projection:

$$L(\omega_0, \omega) = \int\int_{\mathcal{A}_+} R(x; \omega_0, \omega) \langle \omega, \nu(x) \rangle \, d\sigma(x) \equiv \int\int_{\mathcal{P}(\omega, \mathcal{A}_+)} R[P^{-1}(\omega, \mathcal{A}_+, \varkappa); \omega_0, \omega] d^2\varkappa, \tag{7}$$

(R surface scattering model, P^{-1} backprojection $\mathbb{R}^2 \to \mathbb{R}^3$) and its χ^2:

$$\chi^2_L = \sum_i [L^{(\rm obs)}(\omega_{0i}, \omega_i) - L^{(\rm mod)}(\omega_{0i}, \omega_i)]^2 \tag{8}$$

For starlike profiles:

$$\chi^2_\partial = \sum_{ij} [r^{(\rm obs)}_{\rm max}(\alpha_{ij}) - r^{(\rm mod)}_{\rm max}(\alpha_{ij})]^2. \tag{9}$$

In general:

$$\chi^2_\partial = \sum_{ij} \inf_s \Big\{ \|\partial \mathcal{O}_i(s) - \varkappa_{ij}\|^2 \Big\}, \tag{10}$$

$\varkappa_{ij}$ observed profile points, $\partial\mathcal{O}$ modelled profile.

Regularization by, e.g., smoothness:

simple one for low regularization weight:

$$g_S = \int_{\mathcal{B}} [r - \langle r \rangle]^2 \, d\sigma, \tag{11}$$

For higher weights, suppress local concavities:

$$\mathcal{C} = \frac{1}{\sum_i A_i} \sum_{ij} A_{ij} (1 - \langle \nu_i, \nu_{ij} \rangle), \tag{12}$$

where A_i denotes the area of the facet i, and A_{ij} the areas of those facets around it that are tilted above its plane.

Physical constraint: principal axis rotation

$$g_I = (1 - \cos^2 \tau)^2 = [1 - I_3(\mathcal{B})^2]^2, \tag{13}$$

where τ is the angle between the z-axis of the model and the eigenvector $I \in \mathbb{R}^3$ (normalized $\langle I, I \rangle = 1$) corresponding to the largest eigenvalue of the inertia matrix I of the model shape $\mathcal{B}$.

Also, we can augment (10) by

$$\lambda \sum_i \frac{1}{C_i} \oint_{\partial \mathcal{O}_i} \inf_{\varkappa \in \{\varkappa_{ij}\}} \left\{ \| \partial \mathcal{O}_i(s) - \varkappa \|^2 \right\} ds, \tag{14}$$

where $C_i = \oint_{\partial \mathcal{O}_i} ds$. This suppresses irregularity on surface parts not projected near the observed profile points.

3 Maximum compatibility estimate

P parameters, D_i data sources

$$\chi^2_{\rm tot}(P,D) = \chi^2_1(P,D_1) + \sum_{i=2}^{n} \lambda_{i-1}\chi^2_i(P,D_i) \quad D = \{D_i, i = 1,\ldots,n\} \tag{15}$$

with nondegenerate solutions for ech data mode:

$$\arg\min \chi^2_i(P) \neq \arg\min \chi^2_j(P), \quad i \neq j$$

Consider first two data sources:

$$\begin{aligned} x(\lambda) &:= \{\chi^2_1 | \min \chi^2_{\rm tot}; \lambda\}, \\ y(\lambda) &:= \{\chi^2_2 | \min \chi^2_{\rm tot}; \lambda\}. \end{aligned} \tag{16}$$

The curve

$$\mathcal{S}(\lambda) := [\log x(\lambda), \log y(\lambda)] \tag{17}$$

is a part of the boundary $\partial\mathcal{R}$ of the region $\mathcal{R} \in \mathbb{R}^2$ formed by the mapping $\chi : \mathbb{R}^p \to \mathbb{R}^2$ from the parameter space $\mathbb{P}$ into χ^2_i-space:

$$\chi = \{\mathbb{P} \to (\log \chi^2_1, \log \chi^2_2)\}, \quad \mathcal{R} = \chi(\mathcal{P})$$

Translate the origin:

$$\begin{aligned} \hat{x}_0 &= \log x(\lambda)|_{\lambda=0} = \log \min \chi^2_1 \\ \hat{y}_0 &= \log y(\lambda)|_{\lambda\to\infty} = \log \min \chi^2_2. \end{aligned} \tag{18}$$

Now we have the optimal point on $\partial\mathcal{R}$:

$$P_0 = \arg\min \Big([\log \chi_1^2(P) - \hat{x}_0]^2 + [\log \chi_2^2(P) - \hat{y}_0]^2 \Big), \tag{19}$$

so we have, with λ as argument,

$$\lambda_0 = \arg\min \Big([\log x(\lambda) - \hat{x}_0]^2 + [\log y(\lambda) - \hat{y}_0]^2 \Big). \tag{20}$$

We call the point P_0 the *maximum compatibility estimate* (MCE), and λ_0 the *maximum compatibility weight* (MCW). MCE *can be determined without* MCW (or λ).

This approach straightforwardly generalizes to n χ^2-functions and $n-1$ parameters λ_i describing the position on the $n-1$-dimensional boundary surface $\partial\mathcal{R}$ of an n-dimensional domain $\mathcal{R}$: the MCE is

$$P_0 = \arg\min \sum_{i=1}^{n} \left[\log \frac{\chi_i^2(P)}{\chi_{i0}^2} \right]^2, \quad \chi_{i0}^2 := \min \chi_i^2(P), \tag{21}$$

and the MCW is

$$\lambda \in \mathbb{R}^{n-1}: \quad \lambda_0 = \arg\min \sum_{i=1}^{n} \left[\log \frac{\hat{\chi}_{i,\mathrm{tot}}^2(\lambda)}{\chi_{i0}^2} \right]^2, \quad \hat{\chi}_{i,\mathrm{tot}}^2(\lambda) := \left\{ \chi_i^2 \middle| \min \chi_{\mathrm{tot}}^2; \lambda \right\}. \tag{22}$$

Another scale invariant version of MCE can be constructed by plotting χ_i^2 in units of χ_i^2/χ_{i0}^2 and shifting the new origin to $\chi_i^2/\chi_{i0}^2 = 1$:

$$P_0 = \arg\min \sum_{i=1}^{n} \left[\frac{\chi_i^2(P)}{\chi_{i0}^2} - 1 \right]^2, \quad \lambda_0 = \arg\min \sum_{i=1}^{n} \left[\frac{\hat{\chi}_{i,\mathrm{tot}}^2(\lambda)}{\chi_{i0}^2} - 1 \right]^2. \tag{23}$$

This, however, is exactly the first-order approximation of (21) and (22)

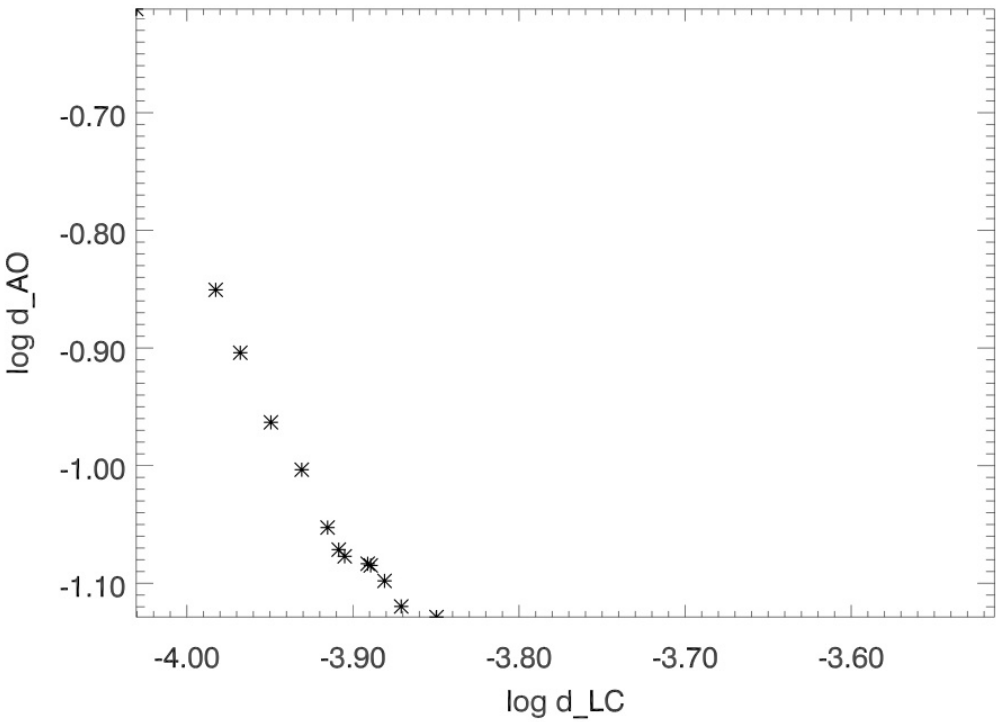

Figure 1: $\mathcal{S}$ curve plotted for 2 Pallas with various weights λ (LC for lightcurves, AO for adaptive optics profiles).

Starlike shapes:

$$r(\theta, \varphi) = \exp\left[\sum_{lm} c_{lm} Y_l^m(\theta, \varphi)\right], \quad (\theta, \varphi) \in S^2 \tag{24}$$

Other shape types by suitable parametrization/mesh.

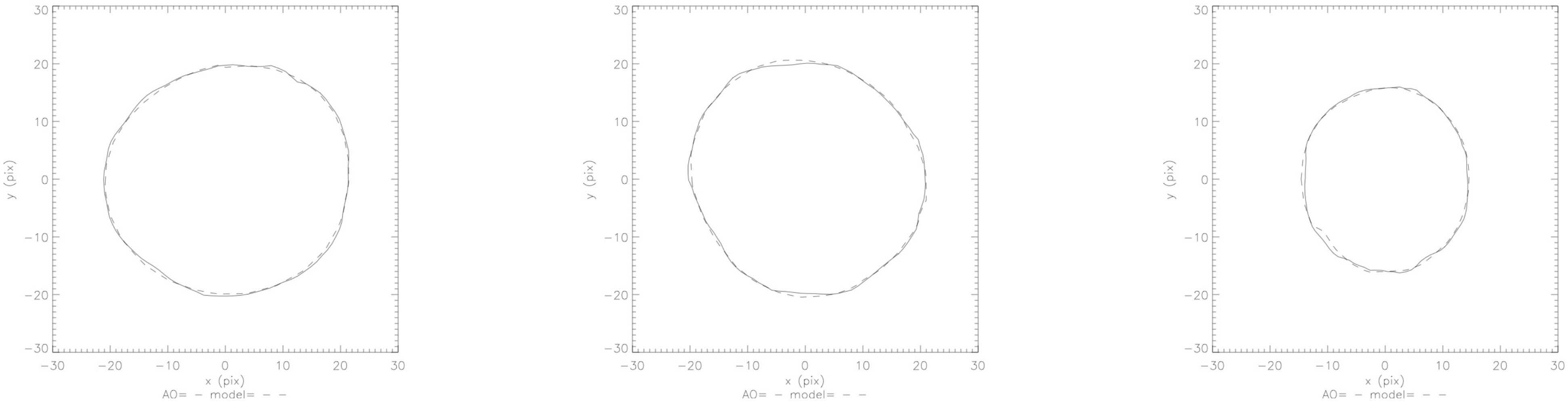

Figure 2: Sample observed (solid lines) vs. modelled (dashed lines) AO contours for 2 Pallas. Coordinates are in pixel units.

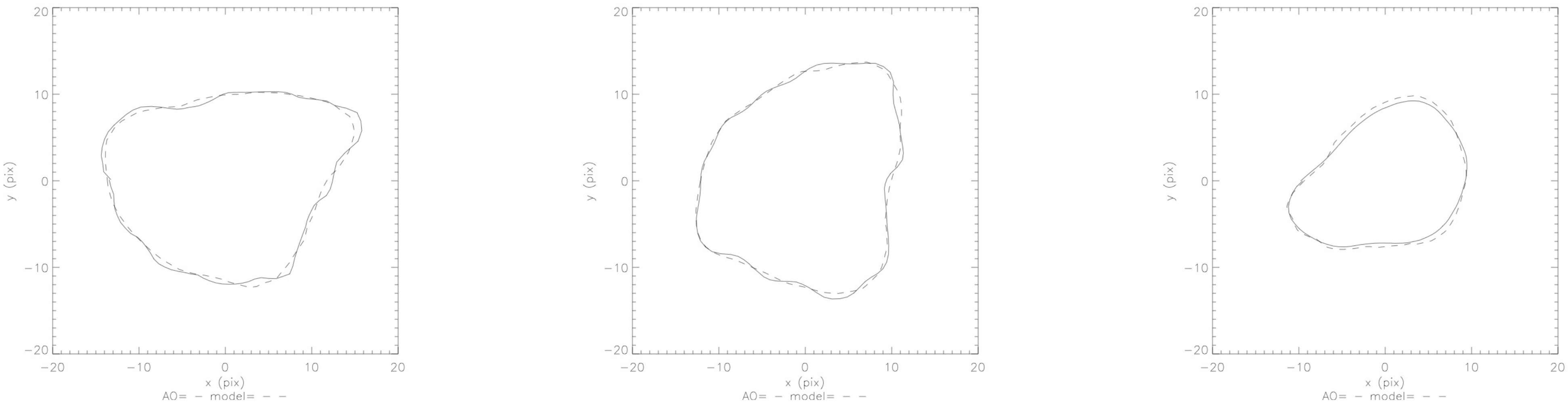

Figure 3: Sample observed (solid lines) vs. modelled (dashed lines) AO contours for 41 Daphne. Coordinates are in pixel units.